Mineralogical Magazine (2024), **88**, 302–311
doi:10.1180/mgm.2024.17

CAMBRIDGE UNIVERSITY PRESS

Article

The mineralogy of the historical Mochalin Log *REE* deposit, South Urals, Russia. Part V. Zilbermintsite-(La), $(CaLa_5)(Fe^{3+}Al_3Fe^{2+})[Si_2O_7][SiO_4]_5O(OH)_3$, a new mineral with ET2 type structure and a definition of the radekškodaite group

Anatoly V. Kasatkin[1], Natalia V. Zubkova[2], Radek Škoda[3], Igor V. Pekov[2], Atali A. Agakhanov[1], Vladislav V. Gurzhiy[4], Dmitriy A. Ksenofontov[2], Dmitriy I. Belakovskiy[1] and Aleksey M. Kuznetsov[5]

[1]Fersman Mineralogical Museum of the Russian Academy of Sciences, Leninsky Prospekt 18-2, 119071 Moscow, Russia; [2]Faculty of Geology, Moscow State University, Vorobievy Gory, 119991 Moscow, Russia; [3]Department of Geological Sciences, Faculty of Science, Masaryk University, Kotlářská 2, 611 37, Brno, Czech Republic; [4]Department of Crystallography, Institute of Earth Sciences, St. Petersburg State University, University Emb. 7/9, 199034 Saint-Petersburg, Russia; and [5]Independent Researcher, Chelyabinsk, Russia

Abstract

The new mineral zilbermintsite-(La), ideally $(CaLa_5)(Fe^{3+}Al_3Fe^{2+})[Si_2O_7][SiO_4]_5O(OH)_3$, was found in a single polymineralic nodule from the Mochalin Log *REE* deposit, Chelyabinsk Oblast, South Urals, Russia. Zilbermintsite-(La) forms anhedral grains up to 0.65 × 0.20 mm at the contact of ferriperbøeite-(La), törnebohmite-(La) and ferriallanite-(Ce). Other associated minerals include bastnäsite-(La), biraite-(La), ferriallanite-(La), ferriperbøeite-(Ce), fluorbritholite-(Ce), monazite-(La), perbøeite-(La), percleveite-(Ce), percleveite-(La), perrierite-(Ce), perrierite-(La), thorianite, thorite and quartz. The new mineral is light brown, translucent in thin fragments with a vitreous lustre. It is brittle, with good {100} cleavage. Mohs hardness is *ca.* 6. D_{calc} = 4.684 g cm^{-3}. Optically, zilbermintsite-(La) is biaxial (+), α = 1.805(7), β = 1.812(7) and γ = 1.867(8) (589 nm); $2V_{meas}$ = 40(15)° and $2V_{calc}$ = 40°. The empirical formula based on $O_{28}(OH,F)_3$ apfu is $(Ca_{0.94}La_{2.56}Ce_{2.18}Nd_{0.20}Pr_{0.10}Th_{0.02})_{\Sigma 6.00}(Al_{2.96}Fe^{3+}_{0.90}Fe^{2+}_{0.64}Mg_{0.34}Mn_{0.13}Ti_{0.03})_{\Sigma 5.00}Si_{7.00}O_{28}[(OH)_{2.42}F_{0.58}]$. Zilbermintsite-(La) is monoclinic, $P2_1/m$; the unit-cell parameters are: a = 8.9605(5), b = 5.7295(2), c = 25.1033(13) Å, β = 116.616(7), V = 1152.21(12) Å^3 and Z = 2. The crystal structure of zilbermintsite-(La) is solved from the single-crystal X-ray diffraction data [R = 0.0757 for 2857 unique reflections with $I > 2\sigma(I)$]. The new mineral is isotypic to radekškodaite-(La) and radekškodaite-(Ce) and together with them forms the newly defined radekškodaite group. All members of this group possess the ET2 type structure where one epidote-type module (E) regularly alternates with two törnebohmite-type modules (T). The new mineral honours Professor Veniamin A. Zilbermints (1887–1939) who was a pioneer of the study of the Mochalin Log deposit. The Levinson suffix-modifier -(La) indicates the predominance of La among rare-earth elements in the mineral.

Keywords: zilbermintsite-(La); new mineral; crystal structure; ET2 type; radekškodaite group; Mochalin Log; South Urals

(Received 23 December 2023; accepted 6 March 2024; Accepted Manuscript published online: 21 March 2024; Associate Editor: Mihoko Hoshino)

Introduction

This article continues a series of papers on the mineralogy and crystal chemistry of new mineral species containing rare-earth elements (*REE*; *lanthanoids* + Y) as species-defining cations (below – '*REE* minerals') discovered at the Mochalin Log deposit, Chelyabinsk Oblast, South Urals, Russia (55°48′42″N, 60°33′46″E). A brief historical outline, the general description, geological and mineralogical data for this deposit were provided in the first paper which also contained the characterisation of two new isostructural gatelite-group minerals, ferriperbøeite-(La) and perbøeite-(La) (Kasatkin *et al.*, 2020a). In the second article we described radekškodaite-(La) and radekškodaite-(Ce), two members of the epidote–törnebohmite polysomatic series with a novel-type structure including one epidote and two törnebohmite modules (ET2) (Kasatkin *et al.*, 2020b). The third paper contained data on the new mineral species percleveite-(La) (Kasatkin *et al.*, 2020c). The fourth paper reported on three new isotypic minerals alexkuznetsovite-(La), alexkuznetsovite-(Ce) and biraite-(La) and the establishment of the biraite group (Kasatkin *et al.*, 2021). Herein we describe another new *REE* mineral from the Mochalin Log deposit that is named zilbermintsite-(La) [Russian cyrilic зильберминцит-(La)] in honour of the outstanding Russian mineralogist and geochemist Professor Veniamin Arkadievich Zilbermints (other spelling: Silberminz) (1887–1939) who worked at the Moscow Mining Academy and in the All-Union Scientific Research Institute of Mineral Resources

Corresponding author: Anatoly V. Kasatkin; Email: anatoly.kasatkin@gmail.com
Cite this article: Kasatkin A.V., Zubkova N.V., Škoda R., Pekov I.V., Agakhanov A.A., Gurzhiy V.V., Ksenofontov D.A., Belakovskiy D.I. and Kuznetsov A.M. (2024) The mineralogy of the historical Mochalin Log *REE* deposit, South Urals, Russia. Part V. Zilbermintsite-(La), $(CaLa_5)(Fe^{3+}Al_3Fe^{2+})[Si_2O_7][SiO_4]_5O(OH)_3$, a new mineral with ET2 type structure and a definition of the radekškodaite group. *Mineralogical Magazine* **88**, 302–311. https://doi.org/10.1180/mgm.2024.17

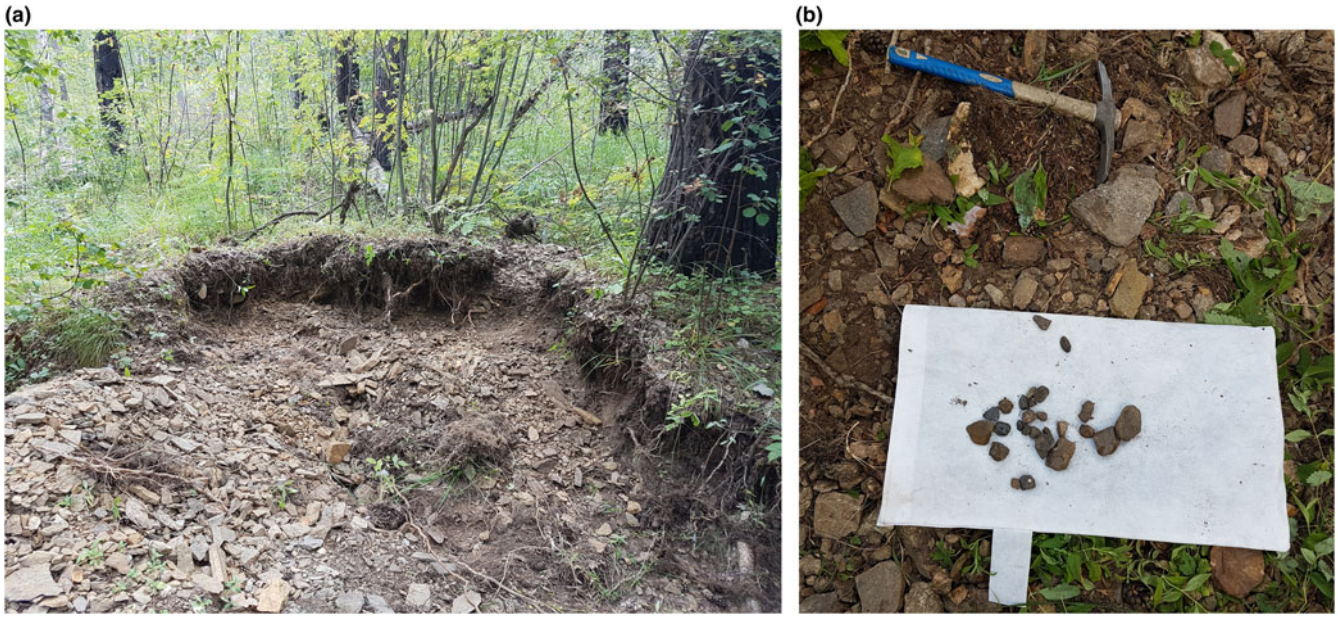

Figure 1. (a) Placer dump no. 2*bis* of the Mochalin Log *REE* deposit where the nodule with zilbermintsite-(La) was collected; (b) freshly collected nodules with numerous *REE*-bearing minerals.

(VIMS), Moscow. In 1927 Prof. Zilbermints discovered an alluvial deposit of rare earth ores in the dumps of an outworked placer gold deposit from the 19th century in the Kyshtym region in the Urals that he called the "cerite deposit" and that is known now as the Mochalin Log *REE* deposit. Based on the results of fieldwork between 1927–1929, Prof. Zilbermints provided detailed geological and petrological description of the deposit, collected and studied numerous *REE*-rich nodules and reported on the main *REE* minerals composing them (Zilbermints, 1928, 1930; Silberminz, 1929). His destiny was tragic: he was falsely accused during Stalin's times, executed and not exonerated for another 20 years. The Levinson modifier -(La) in the mineral name reflects the predominance of La among *REE*. The new mineral, its name and symbol (Zlb-La) have been approved by the Commission on New Minerals, Nomenclature and Classification of the International Mineralogical Association (IMA2023-063, Kasatkin *et al.*, 2023). The holotype specimen is deposited in the systematic collection of the Fersman Mineralogical Museum of the Russian Academy of Sciences, Moscow with the catalogue number 98320.

Occurrence and general appearance

The polymineralic nodule containing zilbermintsite-(La) was collected in August 2018 during fieldwork made by a group of the authors (AVK, RŠ and AMK) at the placer dump no. 2*bis* (Fig. 1). The new mineral occurs as a very few anhedral grains, typically at the contact of ferriperbøeite-(La), törnebohmite-(La) and ferriallanite-(Ce) (Fig. 2). The largest grain found measures 0.65 × 0.20 mm. Apart from the above mentioned species, the very rich *REE* mineral assemblage of this nodule includes bastnäsite-(La), biraite-(La), ferriallanite-(La), ferriperbøeite-(Ce), fluorbritholite-(Ce), monazite-(La), perbøeite-(La), percleveite-(Ce), percleveite-(La), perrierite-(Ce) and perrierite-(La). Non-*REE* bearing minerals present are quartz, thorianite and thorite.

According to the distribution scale of *REE* minerals found at the Mochalin Log deposit (Kasatkin *et al.*, 2020a), zilbermintsite-(La) should be considered as very rare: among 300 nodules with *REE*-bearing minerals investigated by us, it was found in only one of them. In term of its internal structure, this nodule belongs to type 2 (Kasatkin *et al.*, 2020a) where *REE* minerals form thin and chaotic intergrowths with each other. However, the occurrence of zilbermintsite-(La) is restricted to along the contact between törnebohmite-(La) and ferriperbøeite-(La) grains.

Physical properties and optical data

The new mineral is light brown and translucent in thin fragments, with a brown streak and vitreous lustre. It does not fluoresce under ultraviolet light. One direction of good cleavage and one direction of imperfect cleavage were observed under the scanning electron microscope (SEM); from the structure data (see below) we assume that good cleavage could be on {100}. Parting is not observed. Zilbermintsite-(La) is brittle with a fracture stepped in

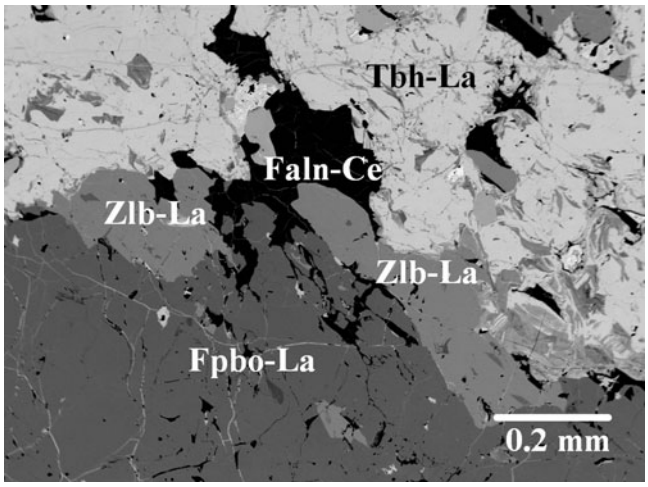

Figure 2. Zilbermintsite-(La) (Zlb-La) closely associated with ferriperbøeite-(La) (Fpbo-La), ferriallanite-(Ce) (Faln-Ce) and törnebohmite-(La) (Tbh-La). Polished section. SEM (BSE) image, specimen no. ML 196-2bis.

https://doi.org/10.1180/mgm.2024.17 Published online by Cambridge University Press

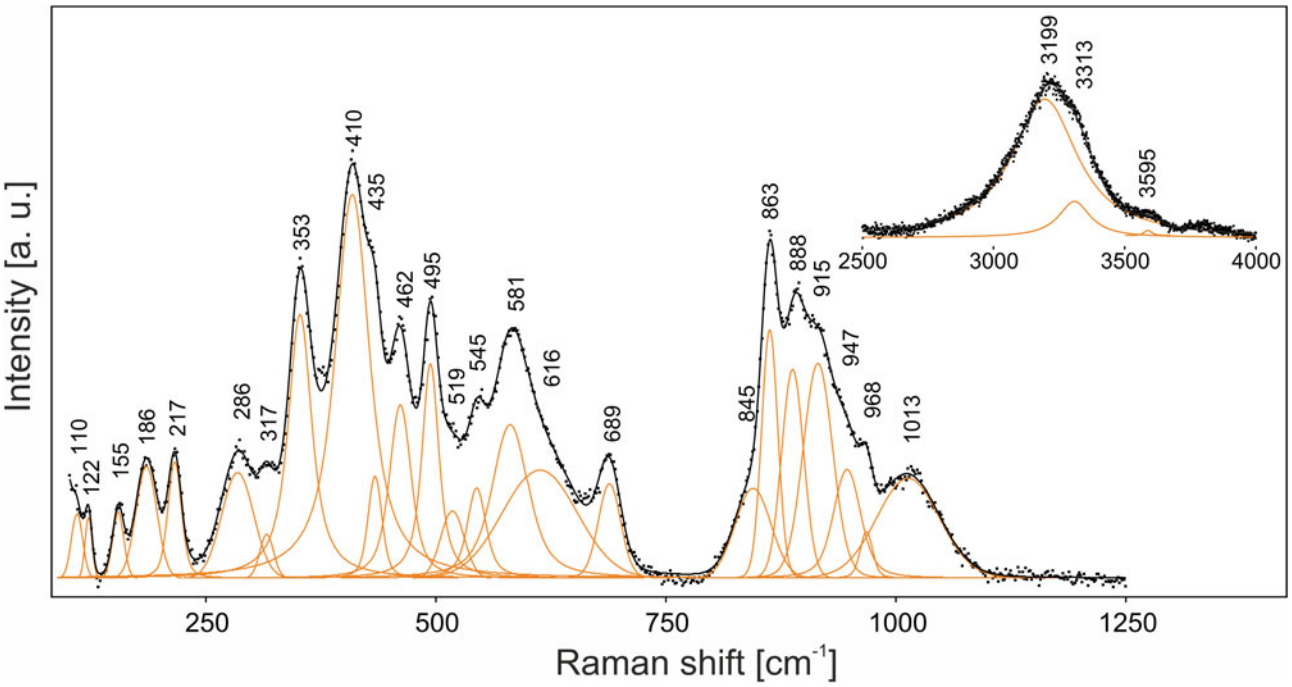

Figure 3. The Raman spectrum of zilbermintsite-(La) excited by 532 nm laser: in the 100–1500 cm^{-1} region and in the 2500–4000 cm^{-1} region (*inset in the upper right corner*). The measured spectrum is shown by dots. The curve matching to dots is a result of spectral fit as a sum of individual Voigt peaks shown below the curve.

the cleavage direction and uneven across it (observed under the SEM). The Vickers micro-indentation hardness (load 150 g) is equal to 838 kg mm^{-2} (range 767–912, $n = 4$) corresponding to *ca.* 6 on the Mohs scale. Density could not be measured due to lack of sufficiently large monomineralic fragments and the absence of heavy liquids with suitable density. A density value calculated using the empirical formula and the unit-cell parameters from single-crystal X-ray diffraction (XRD) data is 4.684 g cm^{-3}.

In transmitted plane-polarised light zilbermintsite-(La) is weakly pleochroic in brown tones. The absorption scheme is $Z > Y > X$. Optically it is biaxial (+), with $\alpha = 1.805(7)$, $\beta = 1.812(7)$, $\gamma = 1.867(8)$ (589 nm), $2V_{meas.} = 40(15)°$ and $2V_{calc.} = 40°$. Dispersion of optical axes is very weak, $r < v$. Optical orientation was not determined due to the anhedral shape of the grains.

Raman spectroscopy

The Raman spectra of zilbermintsite-(La) (Fig. 3) were obtained from polished section by means of a Horiba Labram HR Evolution spectrometer. This dispersive, edge-filter-based system is equipped with an Olympus BX 41 optical microscope, a diffraction grating with 600 grooves per millimetre, and a Peltier-cooled, Si-based charge-coupled device (CCD) detector. After careful tests with different lasers (473, 532 and 633 nm), the 532 nm Nd:YAG diode laser with the beam power of ~5 mW at the sample surface was selected for spectra acquisition to minimise analytical artefacts. A Raman signal was collected in the range of 80–4000 cm^{-1} with a 100× objective (NA 0.9), the system was operated in confocal mode, beam diameter was ~1 μm and the axial resolution ~2 μm. No visual damage of the analysed surface was observed at these conditions after the excitation. Wavenumber calibration was done using the Rayleigh line and low-pressure Ne-discharge lamp emissions. The wavenumber accuracy was ~0.5 cm^{-1} and the spectral resolution was ~2 cm^{-1}. Band fitting was done after appropriate background correction, assuming combined Lorentzian–Gaussian band shapes using the Voigt function.

The assignment of the Raman bands is as follows: bands in the range of 3595, 3313 and 3199 cm^{-1} correspond to O–H-stretching vibrations; 1013 cm^{-1} corresponds to stretching vibrations of Si–O–Si fragments in Si_2O_7 groups; 845 to 968 cm^{-1} to stretching vibrations of apical Si–O bonds; 550 to 700 cm^{-1} are Al–O···H bending vibrations and stretching vibrations of Si–O_b–Si bonds; and 300 to 630 cm^{-1} are due to mixed modes and overlapping bands of (Al,Fe^{3+},Mg)–O-stretching vibrations, as well as bending vibrations of silicate groups. Below 300 cm^{-1} bands are due to lattice modes involving *REE*–O-, Ca–O- and Fe^{2+}–O-stretching vibrations and librational vibrations of silicate groups.

The Raman spectrum of zilbermintsite-(La) is similar to those of radekškodaite-(La) and radekškodaite-(Ce) (Kasatkin *et al.*, 2020b). It is also similar to the spectra of västmanlandite-(Ce) (Holtstam *et al.*, 2005) and ferriperbøeite-(La) (Kasatkin *et al.*, 2020a) in the region of 300–1000 cm^{-1} but differs significantly from them in the region of stretching vibrations of Si–O–Si fragments (1000 to 1100 cm^{-1}) and stretching vibrations involving *REE* and bivalent cations forming low-force-strength bonds (below 300 cm^{-1}). In particular, in the zilbermintsite-(La) spectrum, the bands of stretching vibrations of Si–O–Si fragments are significantly weaker than in the ferriperbøeite-(La) spectrum that reflects a lower Si_2O_7:SiO_4 ratio in the new mineral.

In the Raman spectrum of zilbermintsite-(La), three bands of O–H-stretching vibrations are observed, which corresponds to the number of independent sites occupied by OH groups. The band at 687 cm^{-1} in the Raman spectrum of zilbermintsite-(La) is close to the strong band at 689 cm^{-1} in the Raman spectrum of allanite-(Ce) (Andò and Garzanti, 2014; Čopjaková *et al.*, 2015) and ferriallanite-(Ce) (Sobek *et al.*, 2023) and can be assigned to the symmetric stretching vibrations of Si–O_b–Si bonds of the epidote-type module (Wang *et al.*, 1994).

https://doi.org/10.1180/mgm.2024.17 Published online by Cambridge University Press

Table 1. Chemical composition of zilbermintsite-(La).

Constituent	Wt.%	Range	S.D.	Probe standard
CaO	3.21	3.19–3.24	0.02	Wollastonite
La_2O_3	25.47	25.31–25.88	0.23	$LaPO_4$
Ce_2O_3	21.84	21.75–21.90	0.06	$CePO_4$
Pr_2O_3	1.03	0.98–1.07	0.04	$PrPO_4$
Nd_2O_3	2.01	1.91–2.15	0.09	$NdPO_4$
ThO_2	0.26	0.25–0.28	0.02	$CaTh(PO_4)_2$
MgO	0.84	0.82–0.88	0.02	Mg_2SiO_4
MnO	0.55	0.52–0.57	0.02	Spessartine
Al_2O_3	9.20	8.97–9.30	0.13	Sanidine
FeO*	2.82	6.70–6.85**	0.06**	Almandine
Fe_2O_3*	4.40			
TiO_2	0.14	0.12–0.17	0.02	Anatase
SiO_2	25.68	25.40–25.88	0.24	Sanidine
F	0.67	0.65–0.69	0.02	Topaz
H_2O***	1.33			
–O=F	–0.28			
Total	99.17			

*Total Fe content corresponding to FeO content of 6.78 wt.% was divided into Fe^{2+} and Fe^{3+} based on the occupancies of the *M*1–*M*4 sites found from crystal structure refinement data: see Table 8. Thus, 2.82 wt.% FeO and 4.40 wt.% Fe_2O_3 were calculated based on the found Fe^{2+}: Fe^{3+} atomic ratio: 0.64 Fe^{2+} and 0.90 Fe^{3+} pfu, respectively (Fe^{3+}: Fe^{2+} = 1.40). **For total iron calculated as FeO. ***Calculated by stoichiometry: (OH + F) = 3 apfu. S.D. – standard deviation.

Chemical data

Chemical data (five spot analyses) were obtained using a Cameca SX-100 electron microprobe (WDS mode, acceleration voltage of 15 kV, a beam current of 20 nA and a 3 μm beam diameter). The spectral interference of F*K*α and Ce*M*ζ were manually corrected using empirically determined correction factors. The content of H_2O was not determined directly due to the scarcity of pure material and was calculated by stoichiometry on the basis of $O_{28}(OH,F)_3$ taking into account that bond-valence sums for the O(1), O(2) and O(3) sites are close to 1 (see below). Both the crystal structure and Raman spectroscopy data confirm the presence of OH groups and the absence of B–O, C–O and N–O bonds in the mineral. Analytical data are given in Table 1. Contents of other elements with atomic numbers higher than carbon are below detection limits.

Zilbermintsite-(La) grains are chemically homogeneous and the WDS analyses reveal the uniform chemical composition with only minimal inter-*REE* chemical variation. Lanthanum prevails significantly among *REE* in all analyses. The empirical formula calculated on the basis of $O_{28}(OH,F)_3$ atoms per formula unit (apfu) is $(Ca_{0.94}La_{2.56}Ce_{2.18}Nd_{0.20}Pr_{0.10}Th_{0.02})_{\Sigma 6.00}(Al_{2.96}Fe^{3+}_{0.90}Fe^{2+}_{0.64}Mg_{0.34}Mn_{0.13}Ti_{0.03})_{\Sigma 5.00}Si_{7.00}O_{28}[(OH)_{2.42}F_{0.58}]$.

The ideal formula is $(CaLa_5)(Fe^{3+}Al_3Fe^{2+})[Si_2O_7][SiO_4]_5O(OH)_3$ which requires CaO 3.46, La_2O_3 50.18, FeO 4.43, Al_2O_3 9.43, Fe_2O_3 4.92, SiO_2 25.92, H_2O 1.66, total 100 wt.%.

The Gladstone–Dale compatibility index $(1 - K_p/K_c)$ calculated for zilbermintsite-(La) using its empirical formula and the unit-cell parameters determined from single-crystal XRD data is 0.013 rated as superior (Mandarino, 1981).

Zilbermintsite-(La) does not react with either cold hydrochloric or nitric acid.

Table 2. Powder X-ray diffraction data (*d* in Å) of zilbermintsite-(La).

d_{obs}	I_{obs}	d_{calc}*	I_{calc}**	*h k l*	d_{obs}	I_{obs}	d_{calc}*	I_{calc}**	*h k l*
22.4	**54**	**22.443**	**36**	**0 0 1**	1.929	5	1.931	5	2 0 $\bar{13}$
8.01	**21**	**8.011**	**44**	**1 0 0**			1.926	6	1 2 7
4.661	10	4.660	4	1 1 0	1.871	6	1.869	2	1 0 $\bar{13}$
4.296	10	4.294	2	2 0 4	1.797	14	1.793	4	3 2 $\bar{10}$
4.017	12	4.009	2	2 0 5			1.792	2	5 0 6
3.966	7	4.006	7	2 0 0			1.791	9	2 0 $\bar{14}$
3.742	14	3.741	2	0 0 6	1.763	5	1.767	8	0 2 $\bar{10}$
3.528	9	3.519	3	2 1 3			1.760	2	4 2 $\bar{6}$
3.335	17	3.336	20	2 0 7			1.752	2	4 0 $\bar{13}$
		3.330	5	2 0 2	1.745	18	1.743	15	4 2 3
3.017	**45**	**3.014**	**34**	**2 0 3**			1.668	3	4 0 $\bar{14}$
		2.985	10	3 0 4	1.664	14	1.665	3	2 0 10
2.861	**100**	**2.865**	**100**	**0 2 0**			1.662	2	0 2 $\bar{11}$
		2.863	10	3 0 6	1.648	14	1.643	20	4 2 $\bar{10}$
2.733	**25**	**2.732**	**45**	**2 0 4**	1.611	5	1.610	2	1 2 10
2.704	**26**	**2.698**	**19**	**1 2 0**	1.604	9	1.602	3	5 0 0
2.602	14	2.602	2	1 0 7			1.601	5	2 2 $\bar{13}$
		2.588	8	1 2 4	1.520	4	1.518	9	2 2 $\bar{14}$
2.534	7	2.537	5	1 2 2			1.518	2	5 2 $\bar{7}$
		2.486	2	2 0 5			1.480	5	1 2 $\bar{14}$
2.483	11	2.483	3	1 2 5	1.475	3	1.474	5	6 0 $\bar{10}$
		2.467	3	1 0 $\bar{10}$			1.473	3	5 2 $\bar{10}$
2.431	**20**	**2.424**	**13**	**1 2 3**	1.442	11	1.439	6	4 2 4
2.193	16	2.196	20	4 0 3	1.390	4	1.398	2	5 2 0
2.178	**45**	**2.174**	**35**	**2 2 7**	1.322	6	1.324	2	6 2 $\bar{7}$
2.141	11	2.136	11	0 2 7			1.320	4	0 0 $\bar{17}$
2.077	12	2.076	21	2 2 3			1.319	4	6 2 $\bar{6}$
2.044	11	2.040	2	0 0 $\bar{11}$	1.282	3	1.283	6	4 2 7
		2.025	4	3 2 6	1.269	2	1.269	6	2 4 4
2.012	11	2.013	2	3 0 $\bar{12}$	1.214	4	1.216	2	3 4 $\bar{10}$
		2.006	12	4 0 $\bar{10}$			1.210	2	6 2 0
1.982	16	1.977	29	2 2 4	1.194	2	1.200	3	4 4 $\bar{3}$

*For the calculated pattern, only reflections with intensities ≥2 are given.
**For the unit-cell parameters calculated from single crystal data.
The strongest reflections are given in boldtype.

X-ray crystallography and crystal structure

Powder XRD data were collected using a Rigaku R-AXIS Rapid II single-crystal diffractometer equipped with a cylindrical image

Table 3. Crystal data, data collection information and structure refinement details for zilbermintsite-(La).

Crystal data	
Formula from refinement	$^{A1}(Ca_{0.955}Ce_{0.045})^{A2-6}Ce_5$ $^{M1}(Fe_{0.57}Mg_{0.26}Al_{0.17})^{M2}(Al_{1.87}Fe_{0.13})$ $^{M3}(Fe_{0.75}Mn_{0.15}Mg_{0.10})^{M4}(Al_{0.91}Fe_{0.09})$ $[Si_2O_7][SiO_4]_5O(OH)_3$
Formula weight	1620.40
Temperature (K)	293(2)
Radiation and wavelength (Å)	Mo*K*α; 0.71073
Crystal system, space group, *Z*	Monoclinic, $P2_1/m$, 2
Unit cell dimensions (Å/°)	a = 8.9605(5), b = 5.7295(2), c = 25.1033(13), β = 116.616(7)
V (Å^3)	1152.21(12)
Absorption coefficient μ (mm^{-1})	11.63
F_{000}	1488
Data collection	
Crystal size (mm)	0.04 × 0.13 × 0.16
Diffractometer	Xcalibur S CCD
Absorption correction	Gaussian
θ range (°)	2.723–27.870
Index ranges	$-11 \le h \le 11$, $-7 \le k \le 7$, $-32 \le l \le 33$
Reflections collected	16325
Unique reflections	2857 (R_{int} = 0.0639)
Unique reflections with $I > 2\sigma(I)$	2677
Refinement	
Refinement method	Full-matrix least-squares on F^2
Number of refined parameters	274
Final *R* indices [$I > 2\sigma(I)$]	R_1 = 0.0757, wR_2* = 0.1951
R indices (all data)	R_1 = 0.0811, wR_2* = 0.1994
GoF	1.262
Largest diff. peak and hole, *e*/Å^3	5.59 and –5.48

*$w = 1/[\sigma^2(F_o^2) + (0.1030P)^2 + 21.2454P]$; $P = \{[\max \text{ of } (0 \text{ or } F_o^2)] + 2F_c^2\}/3$.

https://doi.org/10.1180/mgm.2024.17 Published online by Cambridge University Press

Table 4. Atom coordinates and equivalent thermal displacement parameters (U_{eq}, in Å^2) and site occupancy factors (s.o.f.) for zilbermintsite-(La).

Site	s.o.f.	*x*	*y*	*z*	U_{eq}
A(1)	$Ca_{0.955(7)}Ce_{0.045(7)}$	0.2267(4)	¾	–0.06465(14)	0.0162(11)
A(2)	$Ce_{1.00}$	0.59163(11)	¼	0.47069(4)	0.0125(3)
A(3)	$Ce_{1.00}$	0.43319(11)	¾	0.23679(4)	0.0110(3)
A(4)	$Ce_{1.00}$	0.61610(11)	¼	0.17695(4)	0.0119(3)
A(5)	$Ce_{1.00}$	0.77138(15)	¼	0.34770(5)	0.0330(4)
A(6)	$Ce_{1.00}$	0.75178(14)	¼	0.64024(4)	0.0264(3)
M(1)	$Fe_{0.57}Mg_{0.26}Al_{0.17}$*	0	½	0	0.0069(5)
M(2)	$Al_{0.936(16)}Fe_{0.064(16)}$	0.0289(3)	0.4997(5)	0.20902(12)	0.0074(10)
M(3)	$Fe_{0.75}Mn_{0.15}Mg_{0.10}$*	0.3129(3)	¾	0.08724(11)	0.0128(5)
M(4)	$Al_{0.91(2)}Fe_{0.09(2)}$	0	½	½	0.0101(14)
Si(1)	$Si_{1.00}$	0.2044(5)	¼	0.13379(19)	0.0066(8)
Si(2)	$Si_{1.00}$	0.3563(5)	¼	0.29821(18)	0.0053(8)
Si(3)	$Si_{1.00}$	0.7040(5)	¾	0.11733(19)	0.0073(8)
Si(4)	$Si_{1.00}$	0.8405(5)	¾	0.28071(19)	0.0089(8)
Si(5)	$Si_{1.00}$	0.6726(5)	¾	0.40963(19)	0.0072(8)
Si(6)	$Si_{1.00}$	0.1825(5)	¼	0.4256(2)	0.0092(8)
Si(7)	$Si_{1.00}$	0.3440(5)	¼	0.01530(18)	0.0076(8)
O(1) = OH	$O_{1.00}$	0.9239(14)	¼	0.5297(5)	0.010(2)**
O(2) = OH	$O_{1.00}$	0.1064(13)	¾	0.1791(5)	0.007(2)
O(3) = OH	$O_{1.00}$	0.9516(15)	¼	0.2390(5)	0.011(2)
O(4)	$O_{1.00}$	0.0659(15)	¾	0.0561(5)	0.017(3)
O(5)	$O_{1.00}$	0.583(2)	¾	0.3387(6)	0.042(4)
O(6)	$O_{1.00}$	0.2405(10)	0.4905(14)	0.0118(3)	0.0144(16)
O(7)	$O_{1.00}$	0.3735(16)	¼	-0.0435(6)	0.022(3)
O(8)	$O_{1.00}$	0.4875(16)	¼	0.2710(6)	0.025(3)
O(9)	$O_{1.00}$	0.0538(14)	¼	0.4578(5)	0.012(2)
O(10)	$O_{1.00}$	0.9728(14)	¾	0.2501(5)	0.013(2)
O(11)	$O_{1.00}$	0.0921(14)	¼	0.1705(5)	0.011(2)
O(12)	$O_{1.00}$	0.3053(11)	0.4757(15)	0.4440(4)	0.0193(19)
O(13)	$O_{1.00}$	0.8165(10)	0.5146(12)	0.1430(4)	0.0129(16)
O(14)	$O_{1.00}$	0.3297(9)	0.4745(14)	0.1492(3)	0.0098(15)
O(15)	$O_{1.00}$	0.7842(10)	0.5126(13)	0.4332(4)	0.0129(16)
O(16)	$O_{1.00}$	0.7148(11)	0.5256(14)	0.2606(4)	0.0153(17)
O(17)	$O_{1.00}$	0.0551(14)	¼	0.0638(5)	0.015(2)
O(18)	$O_{1.00}$	0.2425(10)	0.4885(13)	0.2765(4)	0.0133(16)
O(19)	$O_{1.00}$	0.5212(14)	¼	0.0722(5)	0.009(2)2
O(20)	$O_{1.00}$	0.5551(18)	¾	0.1367(5)	0.024(3)
O(21)	$O_{1.00}$	0.458(2)	¼	0.3679(6)	0.036(4)
O(22)	$O_{1.00}$	0.5367(19)	¾	0.4344(6)	0.033(4)
O(23)	$O_{0.50}$	0.062(2)	0.320(3)	0.3567(7)	0.017(4)
O(24)	$O_{0.50}$	0.959(2)	0.818(2)	0.3508(7)	0.012(3)

*Fixed during the refinement. For *M*(1) Al *vs* Fe was refined (e_{ref} 20.15), for *M*(3) Fe *vs* Mg was refined (e_{ref} 24.46) (see Table 8). Thus, on the basis of chemical data and e_{ref} *M*(1) site was assumed to be occupied by ($Fe_{0.57}Mg_{0.26}Al_{0.17}$) possibly with minor Ti^{4+} admixture and *M*(3) site by ($Fe_{0.75}Mn_{0.15}Mg_{0.10}$).
**U_{iso}.

Table 5. Anisotropic displacement parameters (in Å^2) in zilbermintsite-(La).

Site	U^{11}	U^{22}	U^{33}	U^{23}	U^{13}	U^{12}
A(1)	0.0244(19)	0.0117(15)	0.0161(17)	0.000	0.0124(13)	0.000
A(2)	0.0075(5)	0.0190(5)	0.0085(5)	0.000	0.0015(4)	0.000
A(3)	0.0074(4)	0.0146(4)	0.0098(5)	0.000	0.0027(3)	0.000
A(4)	0.0087(5)	0.0150(5)	0.0103(5)	0.000	0.0028(4)	0.000
A(5)	0.0160(6)	0.0704(9)	0.0091(5)	0.000	0.0024(4)	0.000
A(6)	0.0173(6)	0.0494(7)	0.0081(5)	0.000	0.0018(4)	0.000
M(1)	0.0034(12)	0.0062(12)	0.0115(12)	0.0004(10)	0.0035(10)	–0.0008(9)
M(2)	0.0045(16)	0.0059(16)	0.0117(17)	0.0003(11)	0.0036(13)	–0.0001(11)
M(3)	0.0089(12)	0.0100(11)	0.0141(12)	0.000	0.0003(10)	0.000
M(4)	0.007(2)	0.008(2)	0.016(2)	0.0013(16)	0.0052(18)	–0.0001(15)
Si(1)	0.0041(18)	0.0059(17)	0.012(2)	0.000	0.0059(16)	0.000
Si(2)	0.0011(18)	0.0036(17)	0.0089(19)	0.000	0.0001(15)	0.000
Si(3)	0.0045(18)	0.0037(17)	0.012(2)	0.000	0.0029(16)	0.000
Si(4)	0.0062(19)	0.0093(18)	0.011(2)	0.000	0.0033(16)	0.000
Si(5)	0.006(2)	0.0056(18)	0.008(2)	0.000	0.0014(16)	0.000
Si(6)	0.006(2)	0.0094(19)	0.013(2)	0.000	0.0048(17)	0.000
Si(7)	0.0069(19)	0.0047(16)	0.0094(18)	0.000	0.0019(15)	0.000
O(2)	0.004(5)	0.004(4)	0.013(5)	0.000	0.004(4)	0.000
O(3)	0.015(6)	0.010(5)	0.010(5)	0.000	0.007(4)	0.000
O(4)	0.015(6)	0.019(6)	0.013(6)	0.000	0.003(5)	0.000
O(5)	0.044(10)	0.068(12)	0.010(6)	0.000	0.010(7)	0.000
O(6)	0.016(4)	0.010(3)	0.019(4)	0.000(3)	0.010(3)	0.001(3)
O(7)	0.021(7)	0.027(7)	0.018(6)	0.000	0.009(5)	0.000
O(8)	0.012(6)	0.043(8)	0.017(6)	0.000	0.004(5)	0.000
O(9)	0.006(5)	0.017(6)	0.014(5)	0.000	0.006(5)	0.000
O(10)	0.004(5)	0.013(5)	0.018(5)	0.000	0.002(4)	0.000
O(11)	0.013(5)	0.016(5)	0.008(5)	0.000	0.009(4)	0.000
O(12)	0.018(4)	0.008(4)	0.037(5)	–0.003(4)	0.017(4)	–0.001(3)
O(13)	0.015(4)	0.003(3)	0.018(4)	–0.002(3)	0.006(3)	0.001(3)
O(14)	0.006(3)	0.015(4)	0.009(3)	–0.002(3)	0.003(3)	–0.002(3)
O(15)	0.010(4)	0.004(3)	0.019(4)	0.003(3)	0.001(3)	0.002(3)
O(16)	0.021(4)	0.008(3)	0.024(4)	–0.002(3)	0.015(4)	–0.003(3)
O(17)	0.008(5)	0.019(6)	0.017(6)	0.000	0.005(5)	0.000
O(18)	0.012(4)	0.003(3)	0.020(4)	0.001(3)	0.004(3)	0.004(3)
O(20)	0.028(7)	0.035(7)	0.009(6)	0.000	0.008(5)	0.000
O(21)	0.028(8)	0.057(10)	0.008(6)	0.000	–0.004(6)	0.000
O(22)	0.024(7)	0.056(10)	0.014(6)	0.000	0.004(6)	0.000
O(23)	0.029(9)	0.008(7)	0.010(7)	0.001(5)	0.007(7)	0.001(6)
O(24)	0.019(8)	0.007(7)	0.016(7)	–0.003(5)	0.013(7)	0.000(5)

plate detector (radius 127.4 mm) using Debye-Scherrer geometry, Co*K*α radiation (rotating anode with VariMAX microfocus optics), 40 kV and 15 mA. Angular resolution of the detector is 0.045°2θ (pixel size 0.1 mm). The data were integrated using the software package *Osc2Tab* (Britvin *et al.*, 2017). Powder XRD data for zilbermintsite-(La) are given in Table 2 in comparison to that calculated from single-crystal XRD data using the *Atoms 5.1* program (Dowty, 2000). Parameters of monoclinic unit cell were calculated from the observed *d* spacing data using *UnitCell* software (Holland and Redfern, 1997) and are as follows: $a = 8.965(4)$, $b = 5.735(3)$, $c = 25.096(9)$ Å, $\beta = 116.68(4)°$ and $V = 1152(8)$ Å^3.

For the single-crystal XRD study, a grain of zilbermintsite-(La), 0.04 × 0.13 × 0.16 mm in size, extracted from the polished section and analysed previously using electron microprobe and Raman spectroscopy, was mounted on a glass fibre and examined with an Xcalibur S single-crystal diffractometer equipped with a CCD detector. A full sphere of three-dimensional data was collected. Data reduction was performed using *CrysAlisPro* software Version 1.171.39.46 (Rigaku Oxford Diffraction, 2018). The data were corrected for Lorentz factor, absorption and polarisation effects.

The crystal structure of zilbermintsite-(La) was solved by direct methods and refined with the use of the *SHELX* software package (Sheldrick, 2015) to $R_1 = 0.0757$ for 2677 unique reflections with $I > 2\sigma(I)$. Two O atoms (O1 and O19) were refined in isotropic approximation of displacement parameters. The crystal data, data collection information and structure refinement details are given in Table 3, atomic coordinates and thermal displacement parameters of atoms in Tables 4 and 5, and selected interatomic distances in Table 6. Bond valence calculations are given in Table 7. Assigned site occupancies (s.o.f.) based on the results of the crystal structure refinement are given in Table 8. The crystallographic information file has been deposited with the Principal Editor of *Mineralogical Magazine* and is available as Supplementary material (see below).

The crystal structure of zilbermintsite-(La) (Fig. 4) consists of the chains of edge-sharing octahedra running along the *b* axis: single chains of the *M*(2)- and *M*(4)-centred octahedra and branched chains with the *M*(1)-centred octahedra in the central part, and the *M*(3)-centred octahedra attached to them from both sides. The chains are linked *via* isolated [SiO_4] tetrahedra

https://doi.org/10.1180/mgm.2024.17 Published online by Cambridge University Press

Table 6. Selected interatomic distances (Å) and angle (°) in the structure of zilbermintsite-(La).

A(1)–O(19)	2.350(11)	*A*(5)–O(8)	2.406(13)	*M*(3)–O(20)	1.958(14)	Si(5)–O(5)	1.593(15)
A(1)–O(13)	2.374(8) ×2	*A*(5)–O(23)	2.546(18)	*M*(3)–O(4)	1.990(13)	Si(5)–O(22)	1.596(16)
A(1)–O(6)	2.388(8) ×2	*A*(5)–O(16)	2.557(8) ×2	*M*(3)–O(14)	2.173(8) ×2	Si(5)–O(15)	1.634(8) ×2
A(1)–O(17)	2.535(12)	*A*(5)–O(15)	2.581(8) ×2	*M*(3)–O(6)	2.261(8) ×2	<Si(5)–O>	1.614
A(1)–O(11)	2.902(12)	*A*(5)–O(9)	2.789(12)	<*M*(3)–O>	2.136		
A(1)–O(7)	3.097(5) ×2	*A*(5)–O(24)	2.971(14)			Si(6)–O(12)	1.625(9) ×2
<*A*(1)–O>	2.612	*A*(5)–O(21)	3.071(17)	*M*(4)–O(1)	1.879(7) ×2	Si(6)–O(23)	1.626(16)
		A(5)–O(5)	3.283(9) ×2	*M*(4)–O(15)	1.911(8) ×2	Si(6)–O(9)	1.680(12)
A(2)–O(21)	2.306(13)	<*A*(5)–O>	2.784	*M*(4)–O(9)	1.965(8) ×2	<Si(6)–O>	1.639
A(2)–O(12)	2.477(9) ×2			<*M*(4)–O>	1.918		
A(2)–O(1)	2.666(12)	*A*(6)–O(22)	2.419(15)			Si(7)–O(19)	1.590(11)
A(2)–O(12)	2.677(9) ×2	*A*(6)–O(12)	2.497(9) ×2	Si(1)–O(14)	1.636(8) ×2	Si(7)–O(7)	1.612(13)
A(2)–O(15)	2.754(8) ×2	*A*(6)–O(24)	2.533(16)	Si(1)–O(11)	1.642(11)	Si(7)–O(6)	1.641(8) ×2
A(2)–O(22)	2.980(4) ×2	*A*(6)–O(18)	2.552(8) ×2	Si(1)–O(17)	1.665(12)	<Si(7)–O>	1.621
A(2)–O(22)	3.075(15)	*A*(6)–O(10)	2.754(12)	<Si(1)–O>	1.645		
<*A*(2)–O>	2.711	*A*(6)–O(23)	2.955(16)				
		A(6)–O(5)	3.267(18)	Si(2)–O(21)	1.570(14)		
A(3)–O(5)	2.295(14)	*A*(6)-O(21)	3.381(9) ×2	Si(2)–O(8)	1.603(14)	disilicate group angle	
A(3)–O(14)	2.521(7) ×2	<*A*(6)–O>	2.799	Si(2)–O(18)	1.645(8) ×2	Si(7)–O(7)–Si(3)	149.6(9)
A(3)–O(2)	2.622(10)			<Si(2)–O>	1.616		
A(3)–O(16)	2.651(9) ×2	*M*(1)–O(4)	1.908(8) ×2				
A(3)–O(18)	2.772(8) ×2	*M*(1)–O(17)	2.037(9) ×2	Si(3)–O(20)	1.612(14)		
A(3)–O(8)	2.967(3) ×2	*M*(1)–O(6)	2.040(8) ×2	Si(3)–O(13)	1.633(8) ×2		
A(3)–O(20)	3.157(13)	<*M*(1)–O>	1.995	Si(3)–O(7)	1.662(13)		
<*A*(3)–O>	2.718			<Si(3)–O>	1.635		
		M(2)–O(13)	1.885(8)				
A(4)–O(19)	2.374(11)	M(2)–O(3)	1.887(8)	Si(4)–O(16)	1.633(9)×2		
A(4)–O(16)	2.454(8) ×2	*M*(2)–O(2)	1.890(7)	Si(4)–O(24)	1.642(16)		
A(4)–O(14)	2.669(8) ×2	*M*(2)–O(18)	1.906(9)	Si(4)–O(10)	1.678(13)		
A(4)–O(3)	2.696(12)	*M*(2)–O(11)	1.947(7)	<Si(4)–O>	1.647		
A(4)–O(13)	2.761(8) ×2	*M*(2)–O(10)	1.958(9)				
A(4)–O(20)	3.005(4) ×2	<*M*(2)–O>	1.912				
A(4)–O(8)	3.055(13)						
<*A*(4)–O>	2.718						

and disilicate groups [Si_2O_7] [the angle Si–O–Si in the disilicate group is equal to 149.6(9)°]. The *A*(1–6) sites occur in large cavities. Even though La^{3+} is a dominant *REE* in zilbermintsite-(La), the Ce^{3+} scattering curve was used during the structure refinement for the *A*(1–6) sites because of the significant content of Ce^{3+} cations, minor amounts of heavier Nd^{3+} and Pr^{3+}, and very minor amount of Th^{4+}. According to the s.o.f. refinement, the *A*(2–6) sites are fully occupied by *REE* cations. The *A*(1) site is Ca-dominant with minor *REE* admixture; Ca *vs* Ce was refined that gave $Ca_{0.955(7)}Ce_{0.045(7)}$. There are four octahedrally coordinated *M* sites, *M*(1–4). For the *M*(1), *M*(2) and *M*(4) sites, Al *vs* Fe was refined, and for the *M*(3) site, Fe *vs* Mg was refined. The *M*(2) and *M*(4) sites are Al-dominant with the refined occupancy $Al_{0.936(16)}Fe_{0.064(16)}$ and $Al_{0.91(2)}Fe_{0.09(2)}$, respectively. These sites centre the smallest octahedra with the mean distances 1.912 Å [*M*(2)–O] and 1.918 Å [*M*(4)–O]. The *M*(1)-centred octahedron is slightly larger, with the mean *M*(1)–O distance of 1.995 Å. This site is Fe^{3+}-dominant, with refined occupancy $Fe_{0.55(2)}Al_{0.45(2)}$, corresponding to number of electrons (e_{ref}) = 20.2(4). On the basis of the chemical information, the *M*(1) occupancy was therefore fixed to $Fe_{0.57}Al_{0.17}Mg_{0.26}$ in the final stage of refinement. The largest *M*(3) octahedron with the mean *M*(3)–O distance of 2.136 Å is predominantly occupied by Fe^{2+} with subordinate Mn, Mg and Fe^{3+} in the atomic ratio Fe^{2+}:Mn:Fe^{3+}:Mg = 0.64:0.15:0.11:0.10, according to both electron microprobe data and refined number of electrons (e_{ref} = 24.46). During the refinement, splitting was found for the O(23) and O(24) sites which deviate from the *m* plane as also occurs in the structures of radekškodaite-(La) and radekškodaite-(Ce).

Bond-valence calculations (Table 7) confirm the above conclusions about distribution of cations between different sites: specifically, Fe^{3+} at *M*(1) and Fe^{2+} at *M*(3).

Discussion

Zilbermintsite-(La) is isotypic to radekškodaite-(La) and radekškodaite-(Ce) (Kasatkin *et al.*, 2020b). They are considered as ET2-type polysomes in which structures can be described as a regular alternation of one module of the epidote-type structure (E) with two modules of the törnebohmite-type structure (T2) (Kasatkin *et al.*, 2020b). Zilbermintsite-(La) differs from radekškodaites by the Fe^{3+} predominance at the *M*(1) site which is Al-dominant in the latter. The E module in zilbermintsite-(La) has ferriallanite-(La) composition whereas in radekškodaite-(La) and radekškodaite-(Ce) it has allanite-(La) and allanite-(Ce) compositions, respectively. According to the mineral group nomenclature (Mills *et al.*, 2009), the radekškodaite group could be established that includes radekškodaite-(La), radekškodaite-(Ce) and zilbermintsite-(La). For their comparison see Table 9.

One of the crucial points for the definition of zilbermintsite-(La) is the distribution of *M* cations including di- and trivalent iron. The arrangement of Fe^{2+}, Fe^{3+}, Al, Mg and Mn between *M* sites is suggested taking into account electron microprobe data (Table 1), refined numbers of electrons (Tables 4 and 8), *M*–O distances (Table 6) and BVS values (Table 7). Unfortunately, we could not determine the valence of iron directly, by means of wet chemical analysis or Mössbauer spectroscopy due to the scarcity of pure material. The methods using

https://doi.org/10.1180/mgm.2024.17 Published online by Cambridge University Press

Table 7. Bond valences for zilbermintsite-(La).

	A(1)	*A*(2)	*A*(3)	*A*(4)	*A*(5)	*A*(6)	*M*(1)	*M*(2)	*M*(3)	*M*(4)	Si(1)	Si(2)	Si(3)	Si(4)	Si(5)	Si(6)	Si(7)	Σ	H-bonding	Σ
O(1)		0.24								$0.56^{\times2\downarrow\ x2\rightarrow}$								1.36	−0.21(O24)	1.15
O(2)			0.27					$0.54^{\times2\rightarrow}$										1.35	−0.14(O4)	1.21
O(3)				0.22				$0.54^{\times2\rightarrow}$										1.30	−0.23(O23)	1.07
O(4)							$0.59^{\times2\downarrow\ x2\rightarrow}$		0.48									1.66	+0.14(O2)	1.80
O(5)			0.63		$0.05^{\times2\downarrow\ x2\rightarrow}$	0.05									1.08			1.86		1.86
O(6)	$0.31^{\times2\downarrow}$						$0.43^{\times2\downarrow}$		$0.25^{\times2\downarrow}$								$0.96^{\times2\downarrow}$	1.95		1.95
O(7)	$0.05^{\times2\downarrow\ x2\rightarrow}$												0.91				1.03	2.04		2.04
O(8)			$0.11^{\times2\downarrow\ x2\rightarrow}$	0.09	0.47							1.06						1.84		1.84
O(9)					0.18					$0.44^{\times2\downarrow\ x2\rightarrow}$						0.87		1.93		1.93
O(10)						0.19		$0.45^{\times2\rightarrow}$						0.87				1.96		1.96
O(11)	0.09							$0.46^{\times2\rightarrow}$			0.95							1.96		1.96
O(12)		$0.39^{\times2\downarrow}$ $0.24^{\times2\downarrow}$				$0.37^{\times2\downarrow}$										$1.00^{\times2\downarrow}$		2.00		2.00
O(13)	$0.32^{\times2\downarrow}$			$0.19^{\times2\downarrow}$				0.54					$0.98^{\times2\downarrow}$					2.03		2.03
O(14)			$0.35^{\times2\downarrow}$	$0.24^{\times2\downarrow}$					$0.35^{\times2\downarrow}$		$0.97^{\times2\downarrow}$							1.91		1.91
O(15)		$0.19^{\times2\downarrow}$			$0.30^{\times2\downarrow}$					$0.51^{\times2\downarrow}$					$0.97^{\times2\downarrow}$			1.97		1.97
O(16)			$0.25^{\times2\downarrow}$	$0.42^{\times2\downarrow}$	$0.32^{\times2\downarrow}$									$0.98^{\times2\downarrow}$				1.97		1.97
O(17)	0.23						$0.43^{\times2\downarrow\ x2\rightarrow}$				0.90							1.99		1.99
O(18)			$0.18^{\times2\downarrow}$			$0.32^{\times2\downarrow}$		0.51				$0.95^{\times2\downarrow}$						1.96		1.96
O(19)	0.34			0.51													1.09	1.94		1.94
O(20)			0.07	$0.10^{\times2\downarrow\ x2\rightarrow}$					0.52				1.03					1.82		1.82
O(21)		0.61			0.09	$0.04^{\ x2\downarrow\ x2\rightarrow}$						1.15						1.93		1.93
O(22)		$0.11^{\times2\downarrow\ x2\rightarrow}$ 0.08				0.46									1.07			1.83		1.83
O(23)					0.36	$0.05^{\times2\downarrow\ x2\rightarrow}$										0.99		1.45	+0.23(O3)	1.68
O(24)					$0.05^{\times2\downarrow\ x2\rightarrow}$	0.37								0.95				1.42	+0.21(O1)	1.63
Σ	2.02	2.79	2.75	2.72	2.54	2.63	2.90	3.04	2.20	3.02	3.79	4.11	3.90	3.78	4.09	3.86	4.04			

Note. Parameters from Gagné and Hawthorne (2015) and, for possible H-bonding, from Ferraris and Ivaldi (1988). The values were calculated taking into account the refined occupancies for the *M*(1–4) and *A*(1) sites. For better clarity the split character of the O(23) and O(24) sites was not taken into account and these sites were considered as averaged with no splitting [the cations–O(23)/O(24) distances for bond-valence calculations including H-bonding were taken for non-split sites]. Slightly low values of BVS for these sites are typical for the members of the radekškodaite group. For Fe cations in the *M*(3) site the bond-valence parameters of Fe^{2+} were used. The bond-valence parameters of Ce^{3+} were used for *A*(1–6) sites. The values of BVS for *A*(2–6) sites could be increased taking into account the presence of La^{3+} cations. Bond valences are calculated disregarding the minor occurrence of F.

Table 8. *M*1–*M*4 sites occupancies (s.o.) suggested for zilbermintsite-(La) based on the results of the crystal structure refinement.

Site	Refined s.o.	SSF_{exp}	Assigned s.o.	SSF_{calc}
*M*1	$Fe_{0.55(2)}Al_{0.45(2)}$	20.15(40)	$Fe^{3+}_{0.57}Al_{0.17}Mg_{0.26}$	20.15
*M*2	$Al_{0.936(16)}Fe_{0.064(16)}$	13.83(22)	$Al_{0.936}Fe^{3+}_{0.064}$	13.83
*M*3	$Fe_{0.89(2)}Mg_{0.11(2)}$	24.46(50)	$Fe^{2+}_{0.64}Mn^{2+}_{0.15}Mg_{0.10}Fe^{3+}_{0.11}$	24.45
*M*4	$Al_{0.91(2)}Fe_{0.09(2)}$	14.17(28)	$Al_{0.91}Fe^{3+}_{0.09}$	14.17

Note. SSF_{exp} and SSF_{calc} are the experimental and calculated site-scattering factors, respectively, normalised to unity.

electron microprobe data (measurement of chemical shift of Fe analytical lines depending on iron valence state) are not effective in this case because of a relatively low content of total Fe in the mineral (*ca.* 5 wt.% Fe). However, the distribution of species-defining Fe^{2+} and Fe^{3+} between the two major iron *M* sites, *M*1 and *M*3, is reliably found from the structure data. The refined numbers of electrons demonstrate that both these sites are Fe-dominant (Tables 4 and 8) and interatomic distances show that the *M*1 site contains Fe^{3+} (*M*1–O = 1.995 Å) whereas Fe^{2+} is concentrated in *M*3 (*M*3–O = 2.136 Å): Table 6. This conclusion is clearly confirmed by bond valence calculations: the BVS values for *M*1 and *M*3 are 2.90 and 2.20 valence units, respectively (Table 7). Finally, the correctness of the site occupancies given in Table 8, as well as the Fe^{2+}:Fe^{3+} ratio found, are confirmed by the lowest value of the Gladstone–Dale compatibility index.

The genetic position of zilbermintsite-(La) respects the general geochemical and crystal chemical trend in the mineral assemblage of some zonal *REE* nodules from Mochalin Log deposit. The *REE* content decreases and the silicate (Si, Al, Fe, Mg and Ca) content increases from central parts of the nodules outwards. The occurrence of zilbermintsite-(La) is situated at the contact between törnebohmite-(La) and ferriperbøeite-(La) and it is in accordance with the generalised genetic sequence (centre to rim) of the epidote–törnebohmite polysomatic series: törnebohmite → radekškodaite/zilbermintsite → perbøeite/ferriperbøeite → allanite/ferriallanite → *REE*-rich epidote. This mineral assemblage also

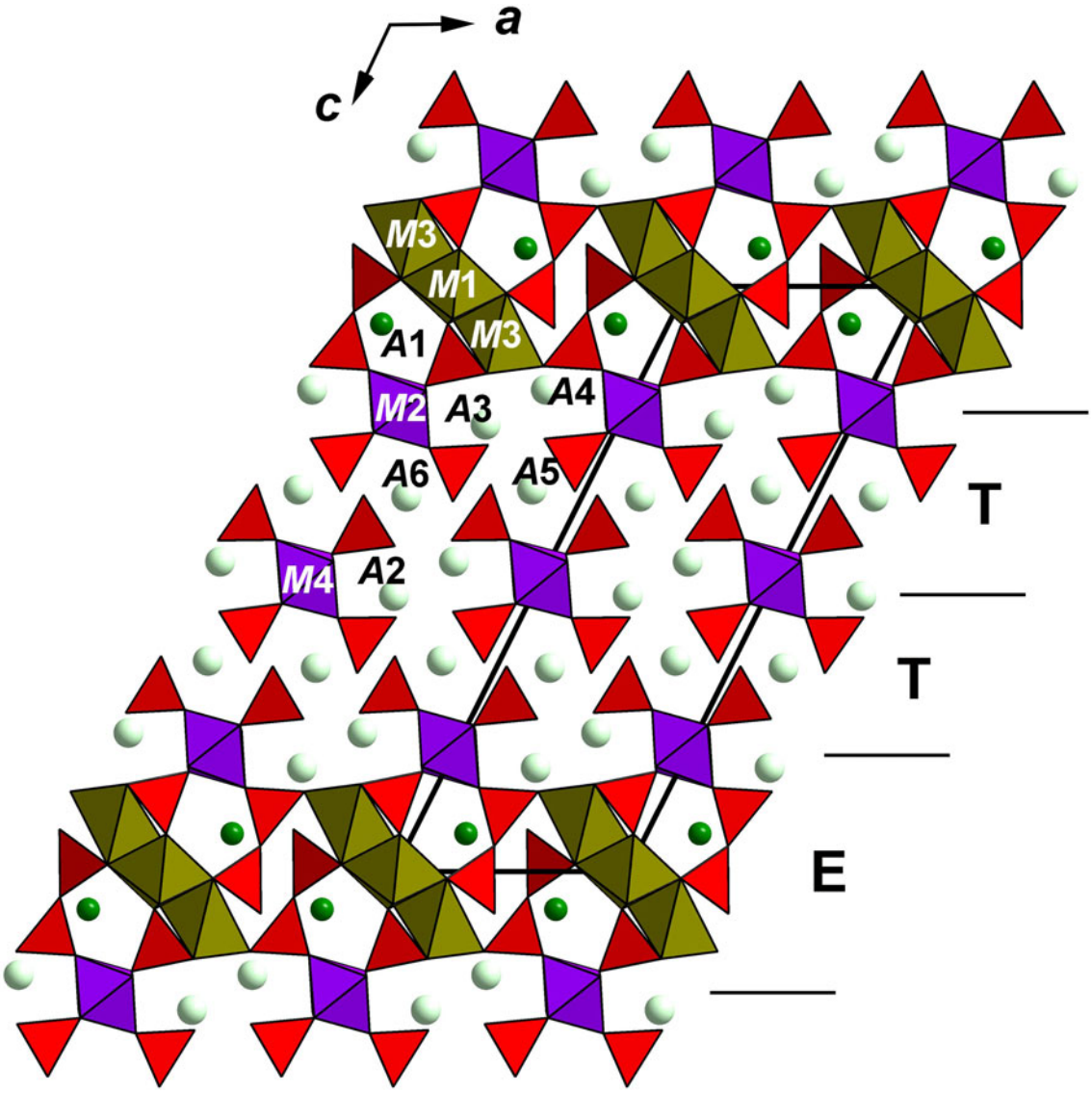

Figure 4. The crystal structure of zilbermintsite-(La). SiO_4 tetrahedra are red. Alternation of epidote-type slabs (E) and törnebohmite-type slabs (T) is shown. The unit cell is outlined. Drawn using *Diamond* version 3.2. (Crystal Impact, 2014).

https://doi.org/10.1180/mgm.2024.17 Published online by Cambridge University Press

Table 9. Comparative data for minerals of the radekškodaite group.

Mineral	Zilbermintsite-(La)	Radekškodaite-(La)	Radekškodaite-(Ce)
Ideal formula	$(CaLa_5)(Fe^{3+}Al_3Fe^{2+})[Si_2O_7][SiO_4]_5O(OH)_3$	$(CaLa_5)(Al_4Fe^{2+})[Si_2O_7][SiO_4]_5O(OH)_3$	$(CaCe_5)(Al_4Fe^{2+})[Si_2O_7][SiO_4]_5O(OH)_3$
E (epidote-type) block	Ferriallanite-(La)	Allanite-(La)	Allanite-(Ce)
Crystal system	Monoclinic	Monoclinic	Monoclinic
Space group	$P2_1/m$	$P2_1/m$	$P2_1/m$
a, Å	8.9605(5)	8.9604(3)	8.9702(4)
b, Å	5.7295(2)	5.7268(2)	5.7044(2)
c, Å	25.1033(13)	25.1128(10)	25.1642(13)
β, °	116.616(7)	116.627(5)	116.766(6)
V, Å^3	1152.21(12)	1151.98(7)	1149.68(11)
Z	2	2	2
Strongest lines of the powder XRD pattern: *d*, Å – *I*, %	22.4–54 8.01–21 3.017–45 2.861–100 2.733–25 2.704–26 2.178–45	22.1–52 8.01–32 4.661–65 3.522–78 3.038–55 2.866–44 2.640–100	22.5–38 8.08–42 4.640–76 3.528–99 3.031–100 2.844–46 2.654–87
D_{calc}, g cm^{-3}	4.684	4.644	4.651
Optical data:			
Optical sign	Biaxial (+)	Biaxial (+)	Biaxial (+)
α	1.805(7)	1.790(7)	1.798(6)
β	1.812(7)	1.798(5)	1.806(6)
γ	1.867(8)	1.825(8)	1.833(8)
2V (meas.) (°)	40(15)	60(10)	65(10)
Pleochroism	Weak, in brown tones; *Z* > *Y* > *X*	Weak, from marsh green to brown; *Z* > *Y* > *X*	Weak, marsh green; *Z* > *Y* > *X*
Source	This paper	Kasatkin *et al.* (2020b)	Kasatkin *et al.* (2020b)

reflects the changes in the trend of alternation between epidote (E) and törnebohmite (T) modules. The abovementioned mineral sequence can be schematised as T→ET2→ET→E. According to the textural relations observed from dozens of *REE* nodules investigated, the minerals of the epidote–törnebohmite polysomatic series are rather cogenetic and probably their distribution mirrors the different activity of *REE* and the other necessary elements (Si, Al, Fe, Ca, Mg, etc) in different parts of the nodules during crystallisation.

Acknowledgements. We thank Associate Editor Mihoko Hoshino, Referee Pietro Vignola and two anonymous reviewers and Principal Editor Stuart Mills for constructive comments that improved the manuscript. The PXRD studies have been performed at the X-ray Diffraction Centre of St. Petersburg State University.

Supplementary material. The supplementary material for this article can be found at https://doi.org/10.1180/mgm.2024.17.

Competing interests. The authors declare none.

References

Andò S. and Garzanti E. (2014) Raman spectroscopy in heavy-mineral studies. *Geological Society of London, Special Publications*, **386**, 395–412.

Britvin S.N., Dolivo-Dobrovolsky D.V. and Krzhizhanovskaya, M.G. (2017) Software for processing the X-ray powder diffraction data obtained from the curved image plate detector of Rigaku RAXIS Rapid II diffractometer. *Zapiski Rossiiskogo Mineralogicheskogo Obshchestva*, **146**, 104–107 [in Russian].

Čopjaková R., Škoda R., Vašinová Galiová M., Novák M. and Cempírek, J. (2015) Sc- and REE-rich tourmaline replaced by Sc-rich REE-bearing epidote-group mineral from the mixed (NYF plus LCT) Kracovice pegmatite (Moldanubian Zone, Czech Republic). *American Mineralogist*, **100**, 1434–1451.

Crystal Impact (2014) *Diamond – Crystal and Molecular Structure Visualization*. Dr. H. Putz & Dr. K. Brandenburg GbR, Kreuzherrenstr. 102, 53227 Bonn, Germany, http://www.crystalimpact.com/diamond.

Dowty E. (2000) *ATOMS - Atomic Structure Display. Version 5.1*. Kingsport, Indiana, USA.

Ferraris G. and Ivaldi G. (1988) Bond valence *vs.* bond length in O···O hydrogen bonds. *Acta Crystallographica*, **B44**, 341–344.

Gagné O.C. and Hawthorne F.C. (2015) Comprehensive derivation of bond-valence parameters for ion pairs involving oxygen. *Acta Crystallographica*, **B71**, 562–578.

Holland T.J.B. and Redfern S.A.T. (1997) Unit cell refinement from powder diffraction data: the use of regression diagnostics. *Mineralogical Magazine*, **61**, 65–77.

Holtstam D., Kolitsch U. and Andersson U.B. (2005) Västmanlandite-(Ce) – a new lanthanide- and F-bearing sorosilicate mineral from Västmanland, Sweden: description, crystal structure, and relation to gatelite-(Ce). *European Journal of Mineralogy*, **17**, 129–141.

Kasatkin A.V., Zubkova N.V., Pekov I.V., Chukanov N.V., Škoda R., Polekhovsky Y.S., Agakhanov A.A., Belakovskiy D.I., Kuznetsov A.M., Britvin S.N. and Pushcharovsky D.Yu. (2020a) The mineralogy of the historical Mochalin Log *REE* deposit, South Urals, Russia. Part I. New gatelite-group minerals ferriperbøeite-(La), $(CaLa_3)(Fe^{3+}Al_2Fe^{2+})[Si_2O_7][SiO_4]_3O(OH)_2$, and perbøeite-(La), $(CaLa_3)(Al_3Fe^{2+})[Si_2O_7][SiO_4]_3O(OH)_2$. *Mineralogical Magazine*, **84**, 593–607.

Kasatkin A.V., Zubkova N.V., Pekov I.V., Chukanov N.V., Ksenofontov D.A., Agakhanov A.A., Belakovskiy D.I., Polekhovsky Yu.S., Kuznetsov A.M., Britvin S.N., Pushcharovsky D.Yu. and Nestola F. (2020b) The mineralogy of the historical Mochalin Log *REE* deposit, South Urals, Russia. Part II. Radekškodaite-(La), $(CaLa_5)(Al_4Fe^{2+})[Si_2O_7][SiO_4]_5O(OH)_3$, and radekškodaite-(Ce), $(CaCe_5)(Al_4Fe^{2+})[Si_2O_7][SiO_4]_5O(OH)_3$, two new minerals with a novel-type structure belonging to epidote–törnebohmite polysomatic series. *Mineralogical Magazine*, **84**, 839–853.

Kasatkin A.V., Zubkova N.V., Pekov I.V., Chukanov N.V., Škoda R., Agakhanov A.A., Belakovskiy D.I., Plášil J., Kuznetsov A.M., Britvin S.N. and Pushcharovsky D.Yu. (2020c) The mineralogy of the historical Mochalin Log *REE* deposit, South Urals, Russia. Part III. Percleveite-(La), $La_2Si_2O_7$, a new *REE* disilicate mineral. *Mineralogical Magazine*, **84**, 913–920.

Kasatkin A.V., Zubkova N.V., Pekov I.V., Chukanov N.V., Škoda R., Agakhanov A.A., Belakovskiy D.I., Britvin S.N. and Pushcharovsky D.Yu. (2021) The mineralogy of the historical Mochalin Log REE deposit, South Urals, Russia. Part IV. Alexkuznetsovite-(La), $La_2Mn(CO_3)(Si_2O_7)$,

alexkuznetsovite-(Ce), $Ce_2Mn(CO_3)(Si_2O_7)$, and biraite-(La), $La_2Fe^{2+}(CO_3)(Si_2O_7)$, three new isostructural minerals and a definition of the biraite group. *Mineralogical Magazine*, **85**, 772–783.

Kasatkin A.V., Zubkova N.V., Škoda R., Pekov I.V., Agakhanov A.A., Gurzhiy V.V., Ksenofontov D.A., Belakovskiy D.I. and Kuznetsov A.M. (2023) Zilbermintsite-(La), IMA 2023-063. CNMNC Newsletter 76. *Mineralogical Magazine*, **88**, 105–109, https://doi.org/10.1180/mgm.2023.89

Mandarino J.A. (1981) The Gladstone-Dale relationship. IV. The compatibility concept and its application. *The Canadian Mineralogist*, **41**, 989–1002.

Mills S.J., Hatert F., Nickel E.H. and Ferraris, G. (2009) The standardisation of mineral group hierarchies: application to recent nomenclature proposals. *European Journal of Mineralogy*, **21**, 1073–1080.

Rigaku Oxford Diffraction (2018) *CrysAlisPro Software System, v. 1.171.39.46*, Rigaku Corporation, Oxford, UK.

Sheldrick G.M. (2015) Crystal structure refinement with SHELXL. *Acta Crystallographica*, **C71**, 3–8.

Silberminz V. (1929) Sur le gisement de cerite, de bastnäsite et d'un minéral nouveau la lessingite dans le district minier de Kychtym (Oural). *Comptes Rendus de l'Academie des Sciences de Russie A*, **3**, 55–60 [in French].

Sobek K., Losos Z., Škoda R., Holá M. and Nasdala, L. (2023) Crystal chemistry of ferriallanite-(Ce) from Nya Bastnäs, Sweden: Chemical and spectroscopic study. *Mineralogy and Petrology*, **117**, 345–357.

Wang A., Han J., Guo L., Yu J. and Zeng, P. (1994) Database of standard Raman spectra of minerals and related inorganic crystals. *Applied Spectroscopy*, **48**, 959–968.

Zilbermints V.A. (1928) The primary deposit of cerite in Kyshtym district. *Mineral'noe syr'e* (*Mineral Raw Materials*), **9/10**, 619–620 [in Russian].

Zilbermints V.A. (1930) The cerite deposit in Kyshtym district (Urals) – in: Rare-earth minerals of Kyshtym area. *Trudy Instituta prikladnoy mineralogii* (*Proceedings of the Institute of Applied Mineralogy*), **44**, 5–42 [in Russian].

https://doi.org/10.1180/mgm.2024.17 Published online by Cambridge University Press